Clim Dyn (2010) 34:185–200
DOI 10.1007/s00382-008-0493-4

The sea ice mass budget of the Arctic and its future change as simulated by coupled climate models

Marika M. Holland · Mark C. Serreze · Julienne Stroeve

Received: 14 July 2008 / Accepted: 11 November 2008 / Published online: 28 November 2008

Abstract Arctic sea ice mass budgets for the twentieth century and projected changes through the twenty-first century are assessed from 14 coupled global climate models. Large inter-model scatter in contemporary mass budgets is strongly related to variations in absorbed solar radiation, due in large part to differences in the surface albedo simulation. Over the twenty-first century, all models simulate a decrease in ice volume resulting from increased annual net melt (melt minus growth), partially compensated by reduced transport to lower latitudes. Despite this general agreement, the models vary considerably regarding the magnitude of ice volume loss and the relative roles of changing melt and growth in driving it. Projected changes in sea ice mass budgets depend in part on the initial (mid twentieth century) ice conditions; models with thicker initial ice generally exhibit larger volume losses. Pointing to the importance of evolving surface albedo and cloud properties, inter-model scatter in changing net ice melt is significantly related to changes in downwelling longwave and absorbed shortwave radiation. These factors, along with the simulated mean and spatial distribution of ice thickness, contribute to a large inter-model scatter in the projected onset of seasonally ice-free conditions.

M. M. Holland (✉)
National Center for Atmospheric Research,
1850 Table Mesa Drive, Boulder,
CO 80305, USA
e-mail: mholland@ucar.edu

M. C. Serreze · J. Stroeve
National Snow and Ice Data Center,
Cooperative Institute for Research in Environmental Sciences,
University of Colorado, Boulder, CO, USA

Keywords Arctic sea ice · Climate change · Climate models

1 Introduction

The Arctic has changed dramatically in recent decades (e.g. Serreze et al. 2000; Overland et al. 2004). Particularly striking is the loss of late summer sea ice (Serreze et al. 2007a). Over the 30-year satellite record (1979–2008), the linear trend in September ice extent is approximately -0.7 million km^2 per decade, equating to a reduction of almost 30%. Extreme seasonal (September) sea ice minima have been observed since 2002 (Serreze et al. 2003; Stroeve et al. 2005). The September minimum of 2007 was particularly dramatic. Ice extent was the lowest ever recorded in the satellite era, and 24% below the linear trend (Stroeve et al. 2008). Ice extent for September 2008 was the second lowest on record, and about 16% below the linear trend. Evidence for attendant thinning of the ice cover in recent decades comes from analysis of upward looking sonar data (Rothrock et al. 1999), reductions in multiyear ice fraction (Nghiem et al. 2006), reductions in ice age (Maslanik et al. 2007) and lengthening of the summer melt season (Belchansky et al. 2004).

Coupled global climate models project continued decreases in sea ice extent and thickness through the twenty-first century (Arzel et al. 2006; Zhang and Walsh 2006; Stroeve et al. 2007; Gerdes and Koberle 2007). In some cases, the simulated loss is quite abrupt and can lead to near ice-free September conditions by the middle of the twenty-first century (Holland et al. 2006). However, rates of loss vary greatly between different models, yielding large uncertainty as to when a seasonally ice-free Arctic Ocean may be realized. Simulated downward trends in

September ice extent over the past 50 years are smaller than observed, suggesting that the models as a group may be conservative regarding their sensitivity to greenhouse gas forcing (Stroeve et al. 2007). Model projections of sea ice conditions through the twenty-first century are being used in a variety of socio-economic and ecological impact assessments (e.g. ACIA 2005). As such, there is an interest in both understanding and reducing the uncertainty associated with these simulations.

Assessing the mechanisms responsible for projected sea ice change and its inter-model scatter requires a closer look at the changing sea ice mass budget. This can aid in the understanding of how thinning of the ice cover translates into increased open water (and decreased ice area) over the melt season. Changes in the ice mass budget are strongly affected by changing ice–ocean–atmosphere heat exchange. Sea ice conditions in turn influence the surface fluxes. Due to different physical representations and parameterizations of sea ice processes, the strength and nature of these interactions likely vary among models (e.g. Holland et al. 2006b).

Here, we examine simulated sea ice mass budgets from 14 coupled global models for an Arctic Ocean domain. These simulations, which are part of the World Climate Research Programme (WCRP) Coupled Model Intercomparison Project, phase 3 (CMIP3; Meehl et al. 2007) archive, were discussed in the Intergovernmental Panel on Climate Change Fourth Assessment Report (IPCC-AR4; IPCC 2007). We first examine climatological mass budgets for late-twentieth century conditions. Attention then turns to projections through the twenty-first century, assessing relationships between evolving ice mass budgets and the surface heat flux which bear on when seasonally ice free conditions are attained. This work represents a step towards understanding and reducing the large scatter in projections between different models. It also offers insight into the mechanisms and feedbacks at work in the Arctic and their importance in shaping the future state of the system.

2 Model simulations

The 14 selected CMIP3 models are listed in Table 1. These models were selected as they all had ice thickness, ice velocity, and atmospheric surface flux information available. The models differ in numerous aspects of their formulation and resolution, but all include dynamic–thermodynamic sea ice components. The output used for this study is available from the Program for Climate Model Diagnosis and Intercomparison (PCMDI). Some of the models have more than one ensemble member. To provide a uniform assessment, we only analyze a single realization (ensemble member) from each model.

Table 1 Sea ice mass budget climatology

Model or data source	Melt	Growth	Divergence	Imbalance	Melt season	Annual mean thickness	Magnitude of annual cycle in thickness
Serreze et al. (2007b)	1.2	1.7	0.3	0.2	JJA		
BCCR	1.7	1.9	0.2	0.0	ASON	2.1	1.7
CCCMa	0.9	1.1	0.2	0.0	JJAS	1.7	0.9
CCCMa-T63	0.7	0.9	0.2	0.0	JJAS	1.7	0.8
CNRM	1.3	1.5	0.2	0.0	JASO	1.5	1.4
GFDL-CM2	1.0	1.1	0.1	0.0	JJAS	0.6	1.0
GISS-AOM	1.5	1.5	0.03	0.0	ASON	1.6	1.5
GISS-ER	1.5	1.6	0.2	−0.1	JJAS	3.5	1.5
Miroc3.2-Med	1.5	1.6	0.1	0.0	JASON	1.8	1.5
MPI-ECHAM5	1.3	1.6	0.3	0.0	JJASO	2.9	1.4
CCSM3	1.0	1.4	0.4	0.0	JJAS	2.3	1.1
HadCM3	1.8	1.9	0.1	0.0	MJJA	1.6	1.9
HadGEM1	1.5	1.7	0.2	0.0	JJA	2.0	1.6
CSIRO-Mk3	0.6	1.2	0.6	0.0	JJAS	3.3	0.8
Miub-ECHOg	1.3	1.4	0.1	0.0	MJJAS	1.5	1.3
Ensemble mean	1.1	1.3	0.2	0.0	JJASO	2.0	1.3
Inter-model SD	0.35	0.31	0.14			0.78	0.33

The annual sea ice mass budget climatology for the Arctic Ocean domain averaged from 1980 to 1999 from the synthesis of Serreze et al. (2007b) based on the historical record, for the individual models and for the multi-model ensemble mean. The mass budget terms are shown in meters of sea ice thickness change per year. The 1980–1999 annual mean ice thickness over this domain (including areas of open water or zero ice thickness) and the magnitude in the annual cycle of ice thickness are also shown in meters. Basic attributes of the models (e.g., resolution, architecture) are available from http://www-pcmdi.llnl.gov/ipcc/model_documentation/ipcc_model_documentation.php

Climate forcings applied over the twentieth century differ for each model. While all include changing greenhouse gas concentrations, they may also include variations in sulfate aerosols, solar input, volcanic forcing, black carbon aerosols, and ozone concentrations. These twentieth century forcings are typically based on observational datasets and chemical transport models. For the twenty-first century, we use integrations which apply the *Special Report on Emission Scenarios* (SRES) A1B forcing (Houghton et al. 2001). This scenario reaches a CO_2 level of 720 ppm by 2100 and is one of the middle range SRES scenarios.

3 Analysis and results

3.1 Sea ice mass budgets

While the public archives from the CMIP3 models include surface radiation and turbulent heat fluxes, they do not include ice melt and growth terms. However, the monthly averaged grid cell ice thickness and ice velocity are available. Using a continuity equation for ice volume:

$$\frac{\mathrm{d}\bar{h}}{\mathrm{d}t} = \Gamma_h - \nabla(\vec{u}h) \tag{1}$$

we are able to compute the relevant terms in the ice mass budget, where $\bar{h}$ is the mean ice thickness, $\vec{u}$ the sea ice velocity, and Γ_h is the thermodynamic source term (i.e., ice melt/growth). This equation is solved for the Arctic Ocean domain shown in Fig. 1 using monthly averaged model output. The mean ice thickness ($\bar{h}$) is computed over this Arctic Ocean domain and is equal to the total ice volume divided by the Arctic domain area. It includes ice-free regions (i.e. areas of zero thickness) within the average. The monthly tendencies in thickness are then assessed using centered differences. The ice thickness divergence (the final term in 1) for the domain is equivalent to the total ice volume transport through transects defining its boundaries. This is computed using the velocity normal to each transect and the effective ice thickness at each transect (h; equal to the thickness over the ice covered portion of the transect multiplied by ice concentration). This includes transects across Fram Strait, Bering Strait, the Barents Sea, and the Canadian Arctic Archipelago (CAA) (the latter when relevant; many models have no open channels through the CAA). Transects are defined on the native model grids and thus the domains differ slightly among the models. The effects of these differences appear to be very small. The thermodynamic source term (Γ_h) in the budget is then solved for as a residual, with its sign indicating whether there is a net thermodynamic gain of ice (positive, referred to as growth) or net thermodynamic loss of ice (negative, referred to as melt) averaged over the domain. In the following discussion, net melt denotes the annual total of all thermodynamic sinks of ice (i.e. melt minus growth). Γ_h includes all thermodynamic sources or sinks of ice volume. For example, the computed ice melt includes contributions from surface, basal and lateral melting. As will be developed, variations in ice growth and melt are related to the surface fluxes, which as mentioned are provided in the CMIP3 archives.

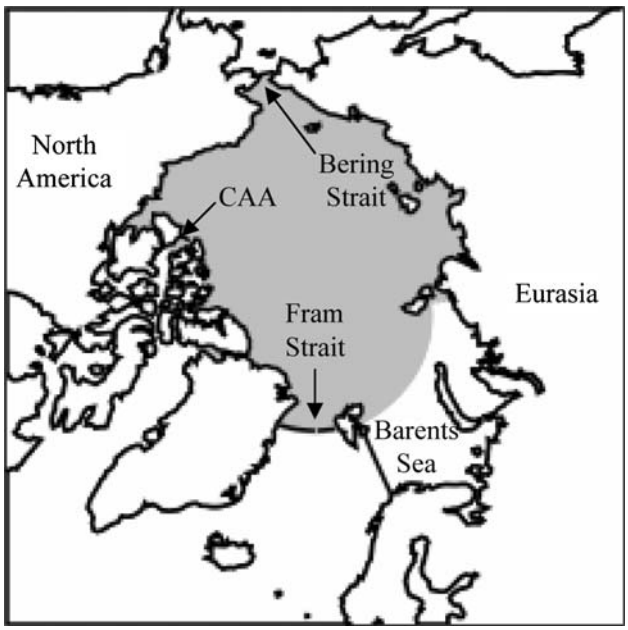

Fig. 1 The Arctic domain used for this study. The Arctic Ocean is defined as the region enclosed by the transects shown by the *solid lines* across Fram Strait, the Barents Sea, the Bering Strait and the Canadian Arctic Archipelago (were relevant, as many models have no open passage there). This is the domain used for the ice mass budget calculations. For the surface heat flux calculations, the Barents Sea is excluded from the analysis and averages are computed over the *shaded region*

The different native models grids, the use of monthly means and calculation of the thermodynamic term as a residual all introduce errors. Nevertheless, our approach represents a reasonable framework for intercomparing results from the various models. Run time diagnostics of the individual sea ice melt and growth terms are available from the Community Climate System Model, version 3 (CCSM3). Values of melt or growth computed from the continuity equation agree very well with this model output with errors of less than 5% on average.

3.2 Ice mass budget climatology

The spatial distribution of annual mean ice thickness from 1980 to 1999 for the 14 models is shown in Fig. 2 along with the multi-model ensemble mean and SD (the right two panels of the last row). As is evident here and also

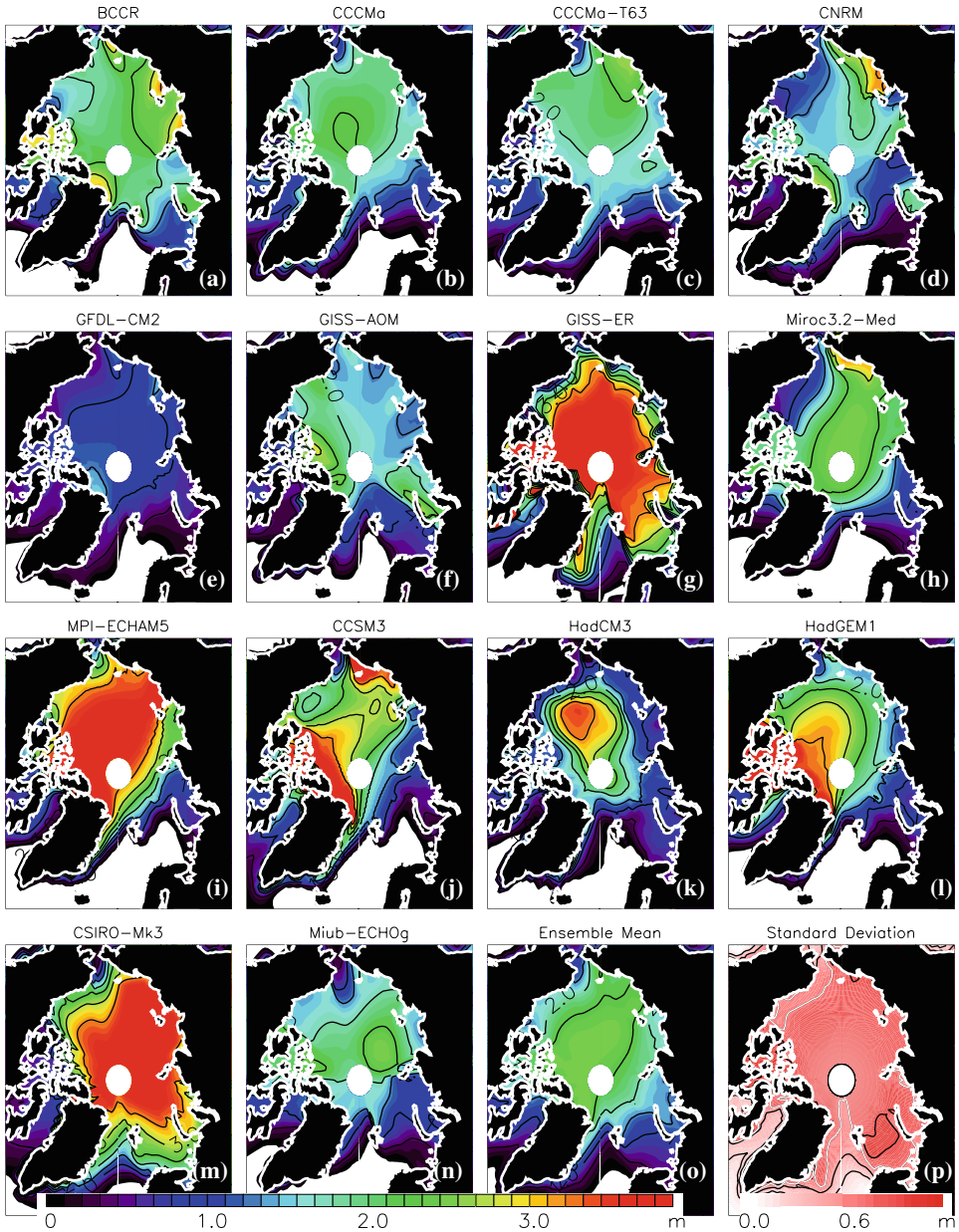

Fig. 2 Climatological late twentieth century annual ice thickness averaged from 1980 to 1999 from the 14 models considered, the multi-model ensemble mean thickness, and the inter-model SD (the latter two as the last two panels of the *bottom row*). The isolines are at intervals of 0.5 m intervals, except for the *bottom right panel*, where the interval is 0.25 m

discussed by Gerdes and Koberle (2007), the Arctic Ocean mean and spatial distribution of ice thickness varies considerably among the models. Available observations (e.g., Bourke and Garrett 1987) show that the thickest ice lies north of the Canadian Arctic Archipelago (exceeding 4 m) with thinner ice along the Eurasian side of the Arctic Ocean (2 m or less). Many models show only small spatial gradients in ice thickness. Others exhibit regions of thinner and thicker ice cover, but not in the right locations compared to observations. Several (notably CCSM3 and UKMO-HadGEM1) show a reasonable thickness pattern. As a result of this scatter, the spatial distribution of thickness in the multi-model mean is unrealistically flat. Within the Arctic basin, the multi-model SD (Fig. 2, bottom right panel) is generally between 0.75 and 1.0 m. The largest scatter is in the Barents Sea, where models range from ice-free conditions (much like observed) to thick (2–3 m) and extensive sea ice.

The late twentieth century (1980–1999) climatological sea ice mass budget for the multi-model ensemble mean is shown in Fig. 3. The ensemble mean melt season, defined as months when the thermodynamic source term is negative, occurs from June to October with a total melt of 1.1 m. Net divergence, primarily through Fram Strait, has a low-amplitude annual cycle and amounts to 0.2 m of annual average ice loss from the Arctic Ocean domain. These sinks are balanced by 1.3 m of ice growth over the period November through May.

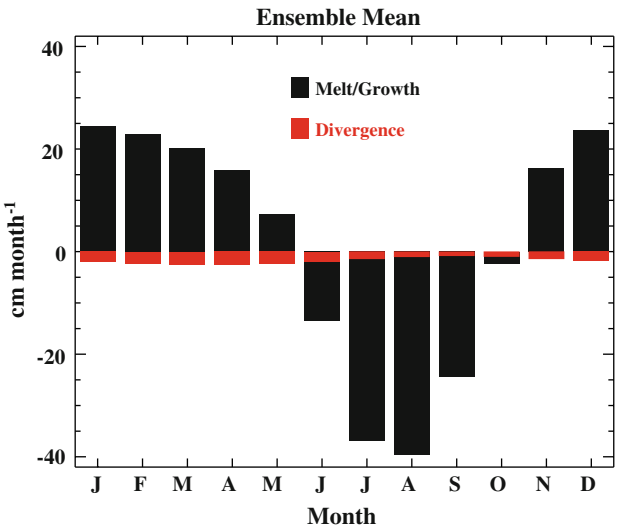

Fig. 3 The annual cycle of the ensemble mean late twentieth century (1980–1999 average) sea ice mass budget

Table 2 Monthly sea ice mass budget

Month	Growth/melt (cm)		Divergence (cm)	
	Serreze et al.	Model	Serreze et al.	Model
Jan	26	25	2	2
Feb	24	23	2	2
March	20	20	3	2
April	16	16	3	3
May	7	7	2	2
June	−31	−12	2	2
July	−54	−36	2	1
Aug	−31	−39	1	1
Sept	6	−24	2	1
Oct	38	−1	2	1
Nov	20	16	2	1
Dec	12	24	3	2

Monthly ice growth/melt and divergence (cm) from the synthesis of Serreze et al. (2007b) based on the historical record and from the ensemble mean of the selected CMIP3 models averaged from 1980 to 1999

Direct observations of sea ice mass budget terms are unfortunately sparse. Serreze et al. (2007b) synthesized a variety of sources to estimate the heat budget averaged over an Arctic Ocean domain almost identical to that in Fig. 1. Data from the European Centre for Medium Range Weather Forecasts ERA-40 reanalysis provided climatological monthly means (1979–2001) of the net surface heat flux (see Sect. 3.3.2 for further discussion). Using hydrographic data to assess climatological monthly changes in ocean sensible heat storage and observations of the latent heat content of the ice divergence term (based on the observed ice volume flux through Fram Strait), they were able to assess the monthly ice growth/melt term as a residual. Using the latent heat of fusion and an assumed ice density of 900 kg m^{-3}, these ice growth/melt and ice divergence terms can be converted from energy units to monthly ice thickness change.

Results from Serreze et al. (2007b) agree with those in Fig. 3 regarding a fairly small and steady ice divergence over the annual cycle and a strongly varying ice growth/melt term (Table 2). The major difference with respect to the model ensemble mean is that the ice melt season lasts three months instead of five, with much stronger melt during June and July. Some caution should be taken when assessing the simulated annual cycle because of the use of monthly averaged data. Satellite imagery clearly shows increasing ice extent (hence ice growth) by the latter half of September. Although little information exists on the seasonal duration and magnitude of basal melting (and thus the length of the net ice melt season), this suggests that the ensemble mean has an ice melt season that extends too far into autumn.

Referring back to Table 1, it is clear that the ice mass budget climatology varies considerably among the 14 models. Six have an ice melt season from June to September. However, in two, the melt season does not begin until August (much later than indicated from observations) while in two, it starts as early as May. The total annual melt varies from 0.6 to 1.8 m among the models, compared to 1.2 m from Serreze et al. (2007b). There is a similarly large range in ice growth (0.9–1.9 m). Ice divergence (i.e., net export) also varies considerably, contributing to an annual Arctic ice loss of between 0.03 and 0.6 m. In general, ice divergence is relatively small compared to ice melt, except in CSIRO-Mk3, for which it equals the annual melt. Differences in melt, growth and divergence result in a large inter-model scatter in the amplitude of the mean annual cycle of ice thickness, with the difference between the seasonal maximum and minimum ranging from 0.8 m in CCCma-T63 and CSIRO-Mk3 to 1.9 m in HadCM3.

In a steady state climate, sea ice achieves an equilibrium annual mean thickness representing a balance between melt, growth and divergence. While for the Arctic Ocean domain considered here, ice divergence is generally the smallest of these terms, it is strongly thickness dependent. This explains much of the inter-model scatter in annual mean ice divergence, which is significantly correlated to the spread in mean Arctic ice thickness at 0.6. Given the same atmospheric forcing, basic sea ice thermodynamics requires that ice growth is also strongly inversely dependant on thickness due to its influence on cold season surface heat loss (e.g. Maykut 1982, 1986). This allows the ice thickness to adjust to the forcing until an equilibrium

mass balance is reached (Bitz and Roe 2004). Given this fundamental property, it is quite surprising that there is no appreciable correlation between inter-model ice thickness and ice growth. The probable explanation is the widely disparate atmospheric forcing simulated by the different models. As a consequence, the ice growth must balance an ice melt and transport that also varies considerably across the models.

Figure 4 shows the correlation and regression of the across-model scatter in the monthly averaged climatological surface heat flux terms and the annual ice melt rates (taken as the total thermodynamic source term for the months when this term is negative). For the late twentieth century climatology, a significant relationship is found between the total ice melt and the net summer surface flux (the sum of the radiative and turbulent fluxes at the surface) from each model. This significant relationship, strongest in July and August when the correlation is about 0.8, is largely due to the contribution of model-to-model differences in the summer net shortwave radiation (correlations with annual ice melt are 0.7 from June through August), with the scatter in the net longwave and net turbulent flux among the models playing a lesser role. Hence, for the climatological mean, models with larger annual melt are generally those in which there is a stronger absorption of shortwave radiation. It follows that the surface albedo feedback is important in driving the model scatter; models with larger annual ice melt generally have a lower summer surface albedo (with the correlation reaching −0.7 for the June albedo). Surface albedo change is primarily responsible for the increased shortwave absorption in these models; inter-model variations in the incident shortwave flux, caused for example by variations in cloud cover, are weak by comparison. No significant correlation emerges between model differences in the monthly averaged net longwave radiation (or its upward and downward components) or the turbulent fluxes and climatological late-twentieth century annual ice melt or growth.

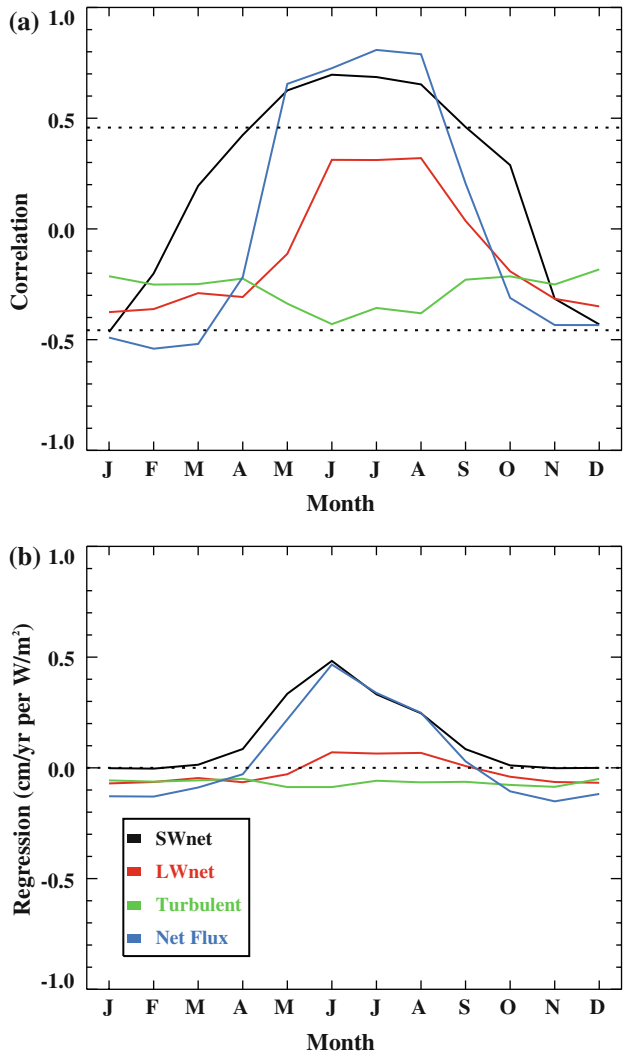

Fig. 4 The (**a**) correlation and (**b**) regression of the across-model scatter in the monthly averaged climatological surface heat flux terms and the annual ice melt rates. The annual ice melt rate is computed as the total annual thermodynamic ice loss as shown in Table 1. The surface heat flux terms are averaged over the domain shown in Fig. 1. The *dashed lines* in panel (**a**) represent the 95% significance level

Pointing to two-way relationships, differences between models in climatological sea ice conditions appear to influence the spread in simulated surface heat fluxes (although this does not explain the inter-model ice growth variations). Models with thicker ice in the annual mean typically simulate less net longwave heat loss at the surface during the cold season months (November through March). This is particularly true for winter (DJF) when the correlation between annual mean thickness and net longwave radiation is 0.7. If the sea ice were primarily responding to the net longwave radiation, thinner ice would be associated with a less negative net longwave budget (less cooling), a negative correlation. Thus, the positive sign of the correlation suggests that ice conditions are influencing the net longwave forcing instead of responding to it. Thicker ice generally inhibits upward heat conduction through the ice, resulting in a lower surface temperature. Interestingly, there is no significant relationship between annual ice thickness and the downward or upward flux components—the relationship only holds with respect to the net longwave flux. The reason is that the surface temperature responds to both the incoming radiation (which has little ice thickness dependence) and the conductive flux through the ice (which is strongly thickness dependent). Consequently, in models with thicker ice, there is less outgoing longwave radiation to counteract the incoming flux, giving rise to a significant relationship only with the net longwave flux.

In summary, for the late twentieth century, sea ice thickness in each model represents an approximate

equilibrium mean annual state, in which annual ice melt is largely balanced by annual ice growth. Net transport to lower latitudes generally plays a smaller role. However, there is large model-to-model scatter in each term. Inter-model variations in the total annual ice melt are strongly related to the absorbed solar flux in summer. Since the cold season surface heat loss (and consequent ice growth) is dependent on ice thickness, the thickness then adjusts until an approximate equilibrium is reached. While scatter in the surface heat flux is related to ice thickness, little relationship exists between annual ice growth and mean ice thickness among the models. The explanation lies in the wide spread among the models in simulated surface fluxes, ice divergence, the spatial distribution of Arctic ice, and other factors not considered here (such as ocean heat exchange).

3.3 Change over the twenty-first century

3.3.1 Ice mass budget change

Many models simulate that considerable Arctic ice loss occurs over the last half of the twentieth century. As such, changes in the simulated ice mass budget are assessed relative to a 1940–1959 reference period. As is clear from Fig. 5a, the multi-model ensemble mean ice thickness decreases considerably over the twenty-first century. Relative to the 1940–1959 average, the ensemble mean ice loss amounts to approximately 1.5 m by 2100. The rate of ice volume loss reaches a maximum during the first half of the twenty-first century and decreases thereafter; a behavior that is also present in other model results (e.g. Arzel et al. 2008). Figure 5b plots the temporal evolution of the contribution to thickness change by ice melt, growth and divergence. Initially, the dominant factor is increased ice melt, with reductions in growth playing a smaller contributing role. After approximately 2050, reductions in ice growth become increasingly important and by the end of the twenty-first century they dominate. In fact, by 2100 less ice melt is simulated than for the mid-twentieth century. This follows in that a considerably thinner ice pack reduces the amount of melt that can be realized. The thermodynamic ice loss is partially compensated by a decrease in ice divergence (meaning a positive contribution to thickness change), which follows as less ice is available to lose via transport to lower latitudes.

Also evident in Fig. 5a and not surprising given earlier discussion, the reduction in ice thickness over the twenty-first century varies considerably across the models. Figure 6 plots the change in annual thickness at the end of the century for the individual models. By the end of the century, thickness changes range from −0.3 m in GFDL-CM2.1 to −2.5 m in CCSM3. The inter-model scatter in

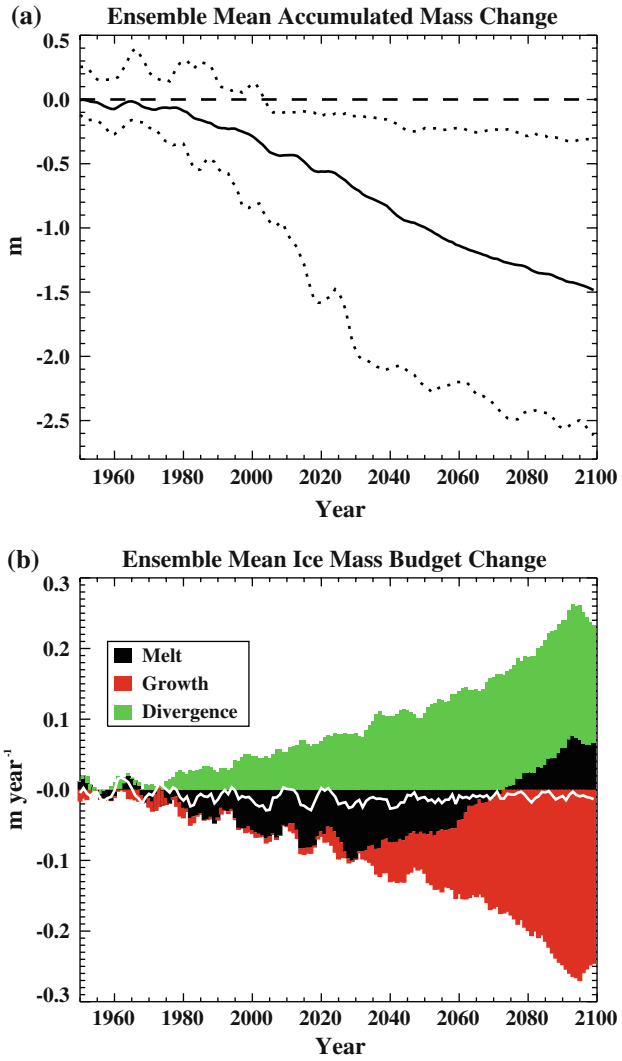

Fig. 5 **a** The accumulated mass budget change (equivalent to the ice volume change) for the multi-model ensemble mean relative to a 1940–1959 time period. The range among different models is shown by the *dotted lines*. **b** Evolution of ensemble mean ice mass budget terms over the twenty-first century relative to the period 1940–1959. Negative values indicate an increasing sink or decreasing source of ice. The *white line* indicates the total change from summing all the mass budget terms, which when accumulated over time gives the ice mass change shown **a**

end of century ice thickness change is in turn highly correlated (at −0.7) with the mid twentieth century ice thickness. In other words, simulations with initially thicker sea ice typically have larger ice volume loss.

The ensemble mean changes in the ice growth, melt and divergence terms plotted in Fig. 5b also mask large model-to-model differences (Fig. 7). Compared to a 1940–1959 baseline, all models project reduced ice transport to lower latitudes (reduced divergence, which considered by itself represents a positive change in the Arctic mass budget and resulting thickness increase). However, by 2050, UKMO-HadCM3, for example, simulates a thickness contribution

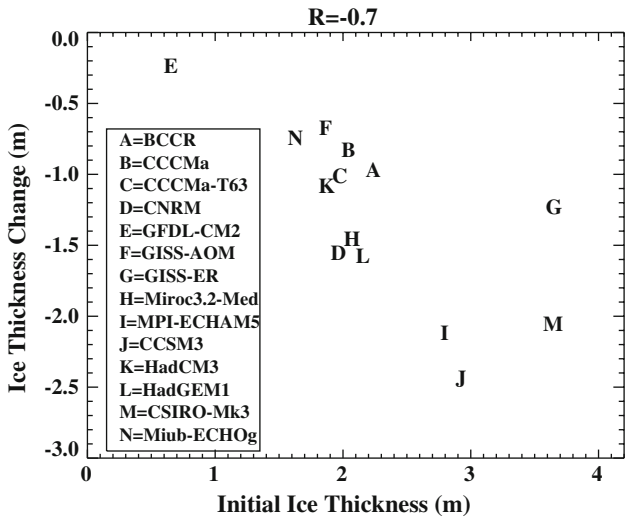

Fig. 6 Scatter plot of the initial (1940–1959) annual ice thickness versus the change in annual ice thickness at the end of the twenty-first century (averaged from 2080 to 2099) for the different models

from reduced ice divergence of only 0.02 m/year whereas in CCSM3 the contribution is 0.36 m/year. The magnitude of the ice divergence change is largely determined by the ice thickness change. As indicated by the strong negative correlation between these two variables ($R = -0.8$), models with a larger decline in ice thickness exhibit a larger decrease in ice divergence. All models simulate a decrease in the net thermodynamic source (growth minus melt) of sea ice over the twenty-first century, which is generally larger in models with initially thicker sea ice. For example, the correlation of inter-model scatter in the net thermodynamic source change at 2100 with respect to the base period and the mid-twentieth century annual ice thickness is -0.6. As indicated by Fig. 7, there is large inter-model scatter not only in the magnitude of the net thermodynamic source change, but also in the relative role of the two terms (melt and growth) that produce it.

There is a strong relationship between the across-model scatter in the changing ice mass budgets and evolving September sea ice extent. Models that retain a more extensive September ice cover through the twenty-first century generally have larger increases in ice melt and smaller reductions (or even small increases) in ice growth. This relationship is maintained throughout the twenty-first century. For 2100 conditions, the across-model scatter in September ice extent is correlated to the scatter in annual ice melt (ice growth) change at -0.8 (0.7). This relationship makes sense in that as models reach nearly ice-free September conditions, they approach the maximum possible ice melt. Further thinning of the ice cover then occurs through reductions in ice growth. This leaves the ice thinner at the onset of the melt season, leading to general reductions in ice melt; a behavior also seen in the ensemble mean.

3.3.2 *The role of changing surface heat budgets*

As has already been established, the late twentieth century and evolving state of the sea ice play important roles in the across-model scatter in the changing twenty-first century sea ice mass budgets. However, the changes in ice melt and growth are ultimately driven by changing atmosphere and ocean heat fluxes. Here we assess changes in the surface heat exchange and the role they play in the across-model scatter in the evolving sea ice mass budgets. Because of limited ocean heat flux information, analysis focuses on changes in the atmosphere–surface heat exchange.

Following Serreze et al. (2007b), the heat budget for an ice–ocean column is:

$$\partial/\partial t(L_\mathrm{i} + S_\mathrm{o} + S_\mathrm{i}) = -\nabla \cdot F_\mathrm{o} + \nabla \cdot F_\mathrm{i} - F_\mathrm{sfc}, \quad (2)$$

where the left hand side is the change in heat storage of the column, including the latent heat storage in floating ice and overlying snow cover (L_i), the sensible heat storage of ocean water (S_o) and the sensible heat storage of sea ice (S_i). This change in heat storage is equal to the sum of the horizontal convergence of the ocean sensible heat flux (F_o), the horizontal divergence of latent heat flux (F_i), and the net surface heat exchange (F_sfc). If we neglect the snow cover component and internal brine pocket melt, the latent heat terms in Eq. 2 can be directly related to ice volume:

$$L_\mathrm{i} \approx -\rho_\mathrm{i} L_\mathrm{f} h, \quad (3)$$

$$F_\mathrm{i} \approx \rho_\mathrm{i} L_\mathrm{f} (\vec{u}h), \quad (4)$$

where ρ_i is the density of ice and L_f the latent heat of fusion. Substituting into Eq. 2 and rearranging then gives:

$$\rho_\mathrm{i} L_\mathrm{f} \left(\frac{\partial h}{\partial t} + \nabla \cdot (\vec{u}h) \right) = \partial/\partial t(S_\mathrm{o} + S_\mathrm{i}) + \nabla \cdot F_\mathrm{o} + F_\mathrm{sfc} \quad (5)$$

If it is assumed that changes in sensible heat storage in the ocean and in sea ice, as well as horizontal ocean heat flux convergence are small (addressed momentarily), the obvious conclusion is that changes in the thermodynamic source term of sea ice (the ice growth or melt, $\Gamma_h = \frac{dh}{dt} + \nabla(\vec{u}h)$, see Eq. 1) are dominated by the evolving net surface heat flux (and its constituent terms). The surface heat flux terms discussed below are averaged over an Arctic regional domain that excludes the Barents Sea (Fig. 1). This is somewhat different than the domain used to compute the sea ice mass budgets. However, it encompasses the region of major ice volume loss that is consistent among the models. Climate models show considerable discrepancies in the simulated atmospheric

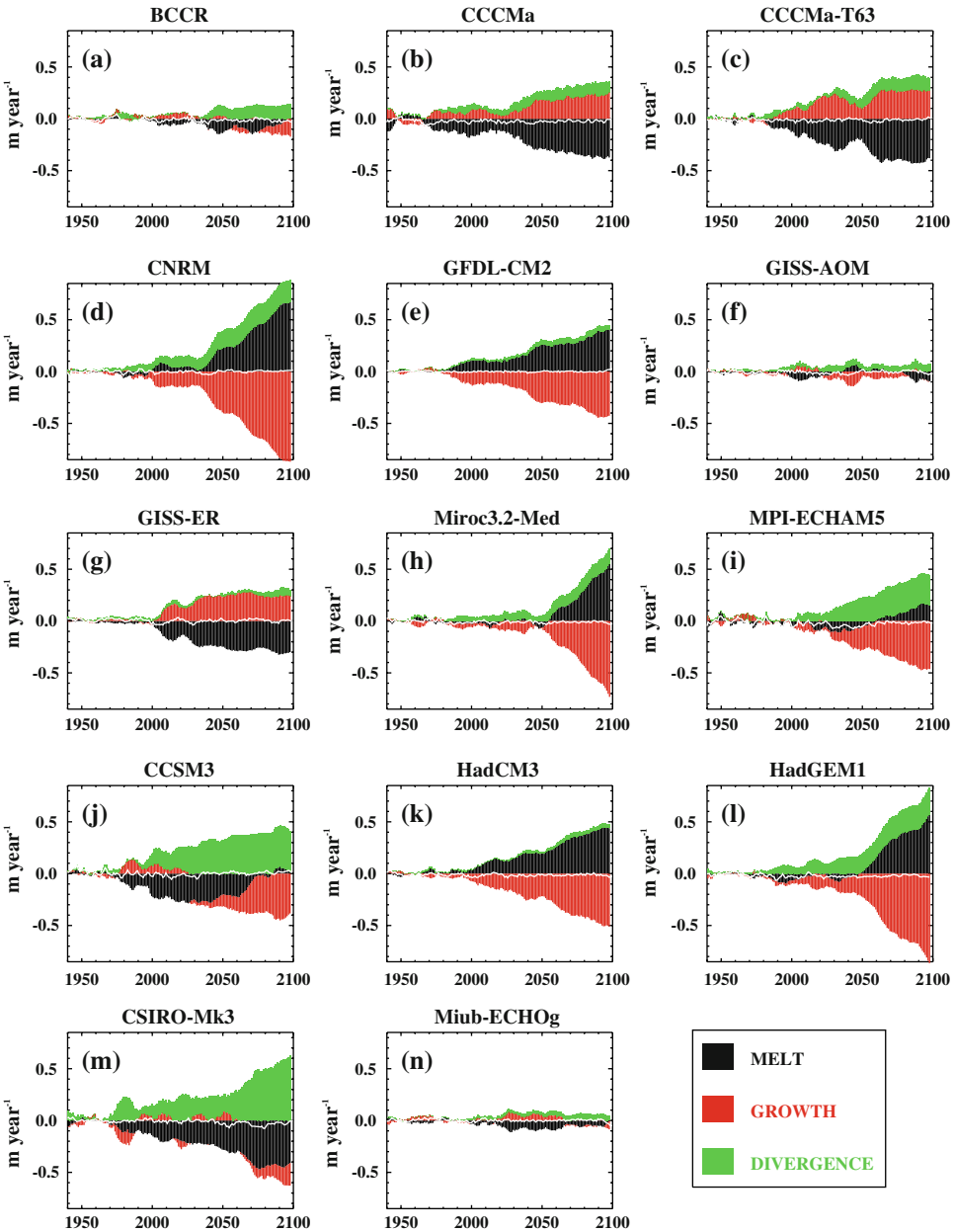

Fig. 7 The ice mass budget change as in Fig. 5b, but for each individual model

conditions over the Barents Sea (Chapman and Walsh 2007). Additionally, the surface heat flux response over the Barents Sea differs considerably to that of the Arctic because, within the twenty-first century, the Barents Sea becomes perennially ice-free in a number of models (Vavrus et al. 2008). As such, we have excluded it from our analysis.

The solid line in Fig. 8 shows the temporal evolution of the correlation between the inter-model spread in net annual atmosphere surface heat flux change and net annual ice melt (melt minus growth) change relative to mid-twentieth century conditions for 13 of the simulations. Specifically, for each year and model, we computed the change in the net annual surface heat flux and in annual ice melt relative to the mid twentieth century, then correlated the 13 paired values. To mitigate noise due to short-term internal variability, the timeseries for each model were first smoothed with a 20-year running mean. Longwave radiation data from the GISS-ER were not available at the time of data processing, so this model is excluded. The correlation is initially strong in the late twentieth century, meaning that models simulating a strong increase in net annual average surface heating tend to be those with strong increases in net ice melt (which is equivalent to strong decreases in the total annual thermodynamic source term). However, the correlations quickly weaken, falling to near zero around 2050. This immediately suggests that the assumption of only small changes in ocean heat flux

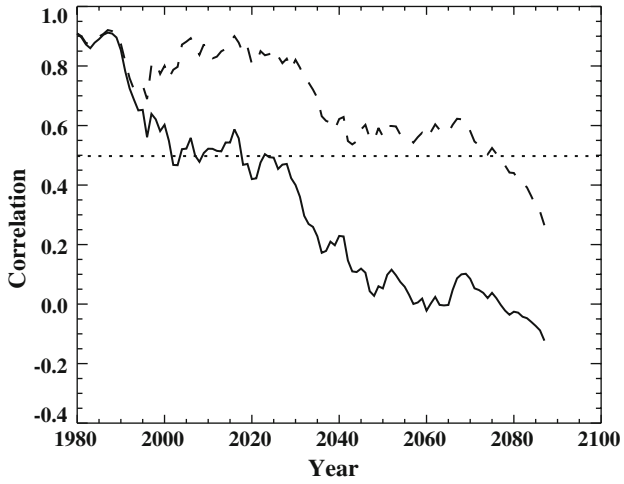

Fig. 8 Time evolution of the correlation of the inter-model scatter in the change in net annual surface heat flux and net annual ice melt (e.g. melt-growth) over the twenty-first century, relative to the 1940–1959 base period. The data are smoothed with a 20-year running mean prior to the computation of the correlations. The sign convention is such that a positive surface heat flux change indicates increased surface heating and a positive net ice melt change indicates a decrease in the thermodynamic ice source term. The *solid line* shows results using 13 models (GISS-ER longwave radiation data was not available and so this model was excluded) and the *dashed line* shows results for a 12-model subset that excludes CCSM3. The *dotted line* indicates the 95% significance level for the 12-model subset

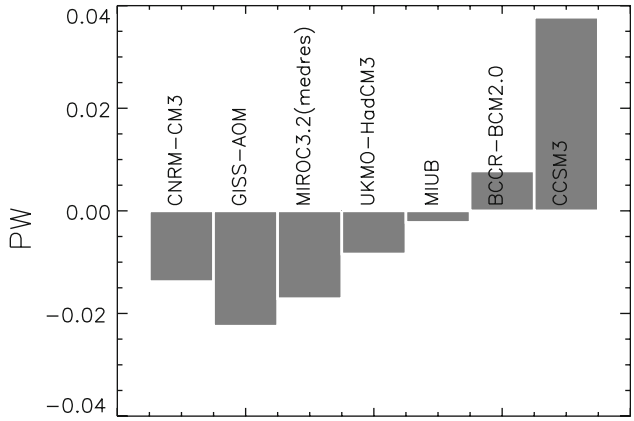

Fig. 9 The change in poleward ocean heat transport at 70°N for a limited model set. The change is computed as the transport averaged for 2040–2049 minus the average for 2000–2009

convergence and sensible heat storage (see discussion above regarding Eq. 5) is incorrect after about the year 2000.

Previous studies (Bitz et al. 2006; Winton 2006; Holland et al. 2006) have documented a substantial increase in ocean heat flux convergence to the Arctic in CCSM3 integrations forced with rising greenhouse gas concentrations. From the limited subset of models for which ocean heat transports are available, it appears that the increase in heat flux convergence in CCSM3 (nearly 0.04 PW) is particularly large, and apart from BCCR-BCM2.0 is the only one exhibiting an increase (Fig. 9). If CCSM3 is excluded, the correlation between changing net surface heat flux and changing net ice melt in the first part of the twenty-first century is much stronger (dashed line in Fig. 8), and remains significant at the 95% level until approximately 2075, after which it weakens considerably. Again this indicates an increasing role for changing horizontal ocean heat flux convergence and sensible heat content. This is not surprising given that a number of simulations reach near September ice-free conditions later in the twenty-first century and likely exhibit larger annually averaged ocean heat content changes after that time.

While the relationship between changes in the net surface heat flux and changes in net ice melt weakens through the twenty-first century, it is still possible that individual terms in the surface heat exchange show a stronger relationship to the across-model variations in the sea ice mass budget changes. Additionally, the evolving sea ice state likely plays a substantial role in the changing surface heat exchange, which can point to important feedbacks at work in the system. An assessment of these factors can suggest where improvements are required in these coupled model simulations in order to improve our capability to project future Arctic ice loss.

Changes in the annual net surface heat flux have contributions from both turbulent and radiative flux anomalies. The annual cycle of mid twenty-first century changes in these terms for each model is shown in Fig. 10. Trends in simulated northern high latitude surface fluxes for the twenty-first century from the CMIP3 models are also discussed by Sorteberg et al. (2007). In general, radiative heating of the surface, primarily during summer, increases through the twenty-first century with a partially compensating increase in heat loss back to the atmosphere via turbulent exchange. The increased summertime radiative heating is largely driven by reductions in albedo. Increasing turbulent heat loss is primarily a cold season phenomenon related to more open water area and greater heat conduction through thinner ice. Changes in net longwave radiation are generally smaller as increases in downwelling longwave radiation are compensated by increases (primarily during the cold season) in the upward longwave heat loss. This pattern and the seasonal cycle of the changing surface heat exchange is one of the classic signals of Arctic amplification. Arctic amplification refers to the idea that rises in surface air temperature through the twenty-first century will be larger over the Arctic Ocean then elsewhere in the northern hemisphere with a distinct cold-season signal (Manabe and Stouffer 1980; Holland and Bitz 2003; Serreze and Francis 2006).

Despite these general conclusions, it is clear from Fig. 10 that the relative importance of change in different

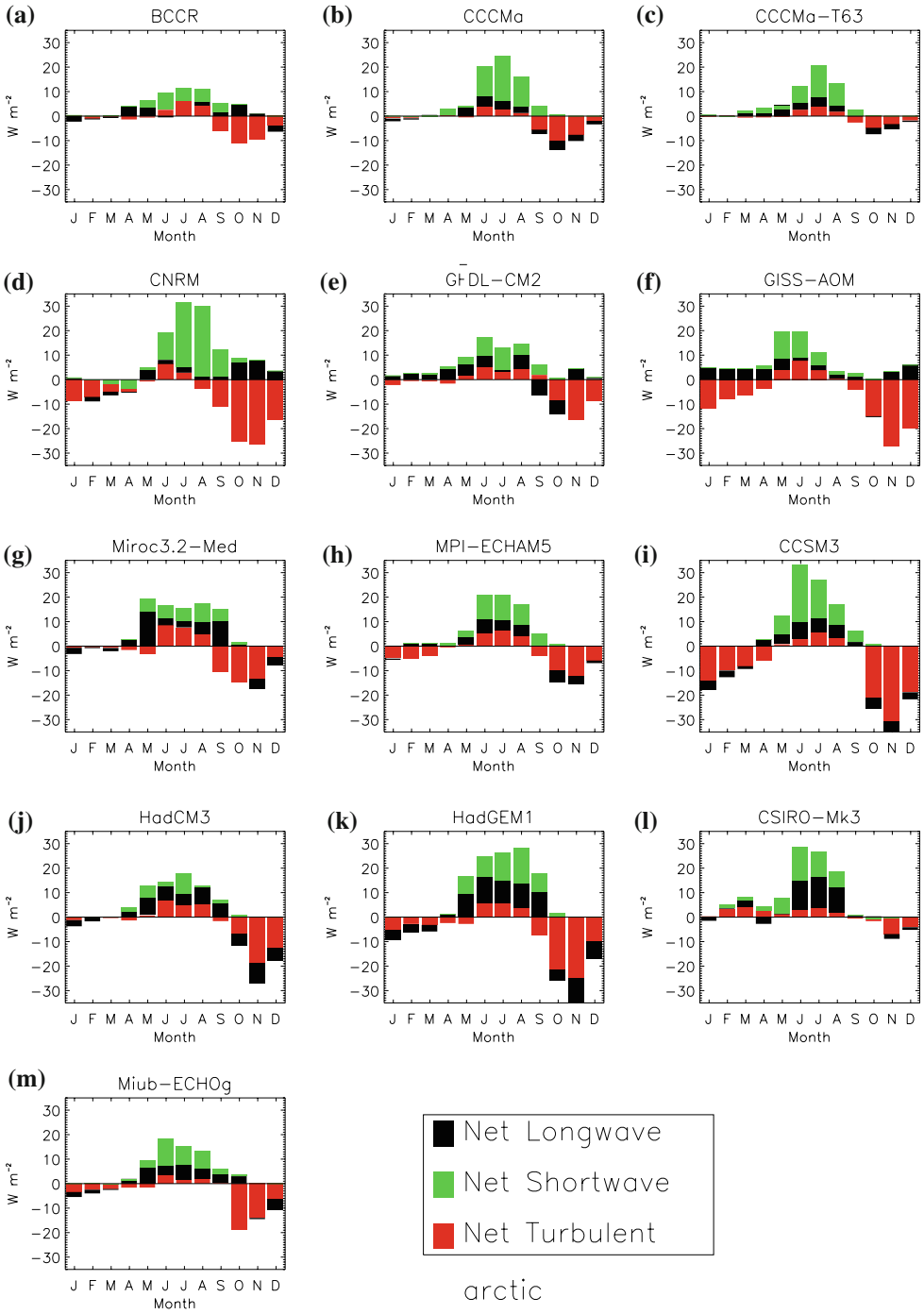

Fig. 10 The mid twenty-first century change in monthly averaged surface heat flux terms for different models shown as the average for 2040–2059 minus the average for 1940–1959. The fluxes are averaged over the domain indicated in Fig. 1 that excludes the Barents Sea. The terms shown are the net longwave flux (*black*), net shortwave flux (*green*) and net turbulent flux (*red*)

terms varies greatly between the models. The initial (mid twentieth century) and evolving sea ice conditions modify the surface heat flux response. For example, because heat conduction through the ice is inversely related to ice thickness, a smaller surface warming should be realized in models with a thicker ice cover. This will have consequent effects on changing turbulent and longwave heat loss (and on the resulting sea ice mass budget). Indeed, the across-model variations in changes in these flux terms are highly correlated to the ice thickness, and models with thicker mid twenty-first century ice generally have smaller increases in the outgoing longwave radiation ($R = 0.8$) and smaller anomalous turbulent heat loss ($R = 0.7$). Sea ice model parameterizations can also influence the changing surface heat exchange. As discussed by Holland et al. (2006b), the inclusion of a subgridscale ice thickness distribution (ITD) can modify the sea ice response and consequent feedbacks in a warming climate. For example, resolving an ITD leads

to larger projected increases in surface turbulent heat loss. Hence it is not surprising that models which explicitly resolve a subgridscale ice thickness distribution (CCSM3, CNRM, UKMO-HadGEM1) also consistently depict large changes in the turbulent heat flux (Fig. 10). Other factors not addressed here include changing cloud conditions and consequent impacts on radiative fluxes and surface temperature change.

Because of the strong coupling between the sea ice conditions and surface heat exchange, it is difficult to isolate the factors responsible for the intermodel scatter in the sea ice mass budget change. However, if we isolate the models with a similar mid twentieth century ice thickness (between 1.5 and 3.0 m, which excludes GISS-ER, CSIRO-mk3.0 and GFDL-CM2.1), there are indications that discrepancies in radiative fluxes are strongly related to the inter-model scatter in ice mass budget change. As summarized in Fig. 11 from correlation analyses for 2050 conditions, larger increases in annual net melting (melt minus growth) tend to occur in models with larger increases in downwelling longwave radiation during the cold season and larger increases in absorbed solar radiation during spring. These same models also generally project larger increases in outgoing longwave radiation and turbulent heat loss, primarily during the cold season. Although cause and effect are difficult to establish, these relationships suggest that inter-model scatter in changing radiative fluxes contributes to the scatter in net ice melt change, with the albedo feedback playing a leading role. The surface fluxes in turn respond to the changing ice conditions and tend to produce larger increases in turbulent and longwave heat loss in models with higher ice volume loss rates and larger surface warming.

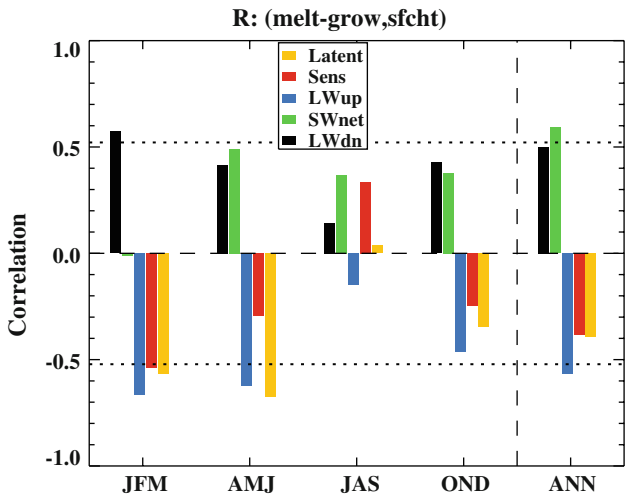

Fig. 11 The correlation of inter-model scatter in surface heat flux changes and annual averaged net ice melt (melt minus growth) change. Only models with a mid twentieth century ice thickness of between 1.5 and 3.0 m are included in this analysis. Correlations are shown for both seasonal and annual surface heat flux values. The changes are computed as the 2040–2059 average minus the 1940–1959 average. The sign convention is such that a positive value indicates that models with larger increases in net ice melt (thermodynamic loss) tend to have larger increases in surface heating for the particular heat flux term. The values shown are correlations for changes in net ice melt with changes in the downwelling longwave (*black*), net shortwave (*green*), outgoing longwave (*blue*), sensible heat flux (*red*) and latent heat flux (*orange*). The *dotted line* indicates the 95% significance level

While all the models project increased downwelling longwave radiation in the twenty-first century, they also project a decrease in downwelling shortwave radiation. This is consistent with a decreasing surface albedo and the consequent decline in multiple scattering between the surface and clouds (e.g. DeWeaver et al. 2008). It is also consistent with increased Arctic cloud cover (fractional coverage) in most simulations, although there is a large scatter in the magnitude and even the sign of this response (Vavrus et al. 2008). As expected, models with larger increases in cloud cover generally exhibit larger increases in downwelling longwave radiation and larger decreases in downwelling shortwave radiation (not shown). Changes in cloud properties (e.g. cloud height, liquid water content, etc.) can also modify the surface radiative flux changes (e.g. Gorodetskaya et al. 2008). An analysis of these effects is beyond the scope of the present paper. Our results do suggest, however, that the inter-model scatter in changing Arctic cloud conditions likely plays an important role in simulated ice melt change.

3.4 Influence on the timing of a seasonally ice free Arctic

With the A1B emissions scenario, a seasonally ice-free Arctic (zero ice extent) is realized in about 50% of the CMIP3 models by 2100 (e.g. Arzel et al. 2006; Zhang and Walsh 2006) with some models reaching near ice-free September conditions as early as 2050. Based on the preceding analyses, the timing of when a seasonally ice-free Arctic is realized in these simulations should be influenced by the initial ice thickness and the changing ice mass budgets. Here we examine the factors that influence the changing ice extent and how they vary among the models.

Figure 12a shows the timeseries of twenty-first century September ice extent from the subset of 14 CMIP3 models. For the models as a group, there is a positive relationship between the simulated late twentieth century ice extent and extent throughout the twenty-first century. There is also a relationship between the simulated annual mean twentieth century ice thickness and projected September ice extent. For example, the inter-model scatter in 2050 September ice extent correlates with the late twentieth century annual mean ice thickness at 0.8 and with the late twentieth

century September extent at 0.9. In other words, and not surprisingly, models with initially thicker, more extensive ice tend to retain more extensive summer ice throughout the twenty-first century. However, the strong relationship between evolving September ice extent and initial annual thickness is due primarily to models with extremely thin or thick initial ice cover. When considering the subset of models with an initial annual mean thickness from 1.5 to 3.0 m, the correlation is weak.

It is instructive to consider the simulated September ice extent as a function of the evolving annual mean ice thickness (instead of time) (Fig. 12b). This gives some indication of how net changes in the sea ice mass budget translate into ice extent loss. In general, the relationship between ice thickness and September extent is nonlinear. In a thick sea ice regime (>2.5 m), considerable ice volume loss can occur with only a small influence on the summer ice extent. However, when the average annual mean Arctic sea ice falls to less then approximately 2 m, appreciable regions of the ice pack can completely melt out in summer, yielding a much larger change in ice extent per ice volume loss. Thus, although models with thicker initial ice typically simulate larger ice volume loss (Fig. 6), this translates into only small changes in the late-summer ice extent. This likely explains why models with thick (greater then 3.0 m) late twentieth century sea ice show only small changes in ice extent through the twenty-first century. It also suggests that discrepancies between the simulated and actual twentieth century sea ice thickness may contribute to the relatively small rates of summer ice extent loss simulated by most models (Stroeve et al. 2007).

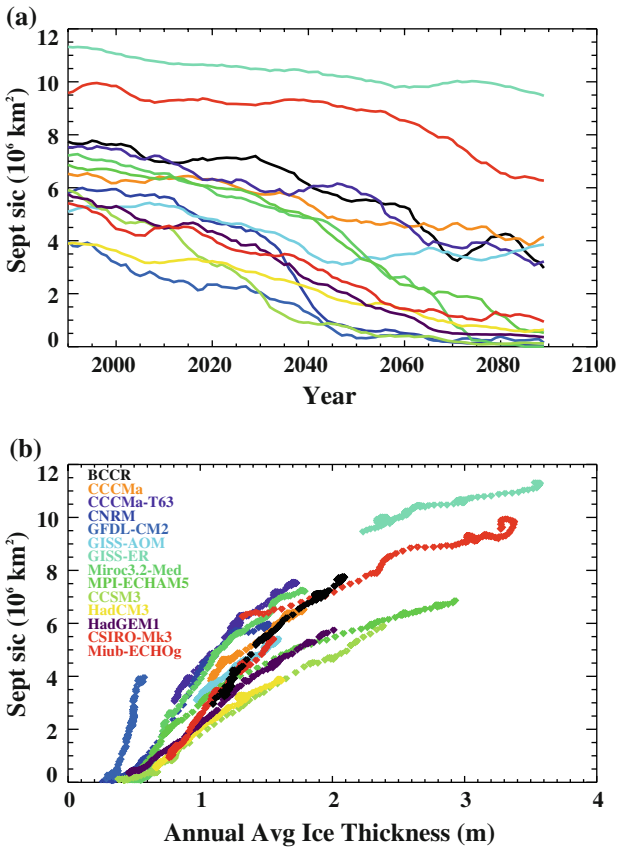

Fig. 12 (**a**) The timeseries of September ice area and (**b**) the twenty-first century September ice area versus the annual average ice thickness for the different models

The slopes of the lines on Fig. 12b also indicate that, for similar annual mean thickness (e.g. from 1 to 2 m), models vary in the September ice extent loss that occurs for an equivalent annual mean thickness change. One important contributor to these differences is the spatial distribution of thickness (Fig. 13). If considering time periods when the simulations have a similar mean ice thickness of approximately 1.2 m, models with a larger rate of September ice retreat per meter of ice thickness change generally have a smaller spread in the distribution of March ice thickness (Fig. 13; upper left panel). This suggests that the distribution of ice at the initiation of the melt season influences how much end-of-summer ice extent loss can occur. While an intriguing relationship, the processes responsible for it are not entirely clear. Perhaps it results from a stabilizing influence of thick ice regions, which reduce the amount of open water formation that can occur for the same ice volume loss. Other factors are also likely to influence the inter-model scatter in the rate of ice retreat per meter of ice thickness change, such as the strength of the albedo (and other) feedbacks.

4 Conclusions and discussion

We have assessed the sea ice mass budgets for the late twentieth century and projections through the twenty-first century in a number of CMIP3 simulations. There is large inter-model scatter in the contemporary mass budget. Annual ice growth and melt range by a factor of greater than two and approximately three, respectively. The length of the melt season varies from three to five months, and in some models extends even into November. While these differences reflect many factors and cause and effect are difficult to assess, variations in the absorbed solar radiation among the models are very important, pointing in turn to differing surface albedo simulations. This likely reflects not only a forcing on the intermodel scatter in ice melt, but also a feedback of enhanced melt onto the surface albedo simulation. The net transport (divergence) of ice out of the Arctic, while generally a smaller term in the climatological mass budget, is also highly variable across the models. This scatter is related most strongly to inter-model variations in ice thickness.

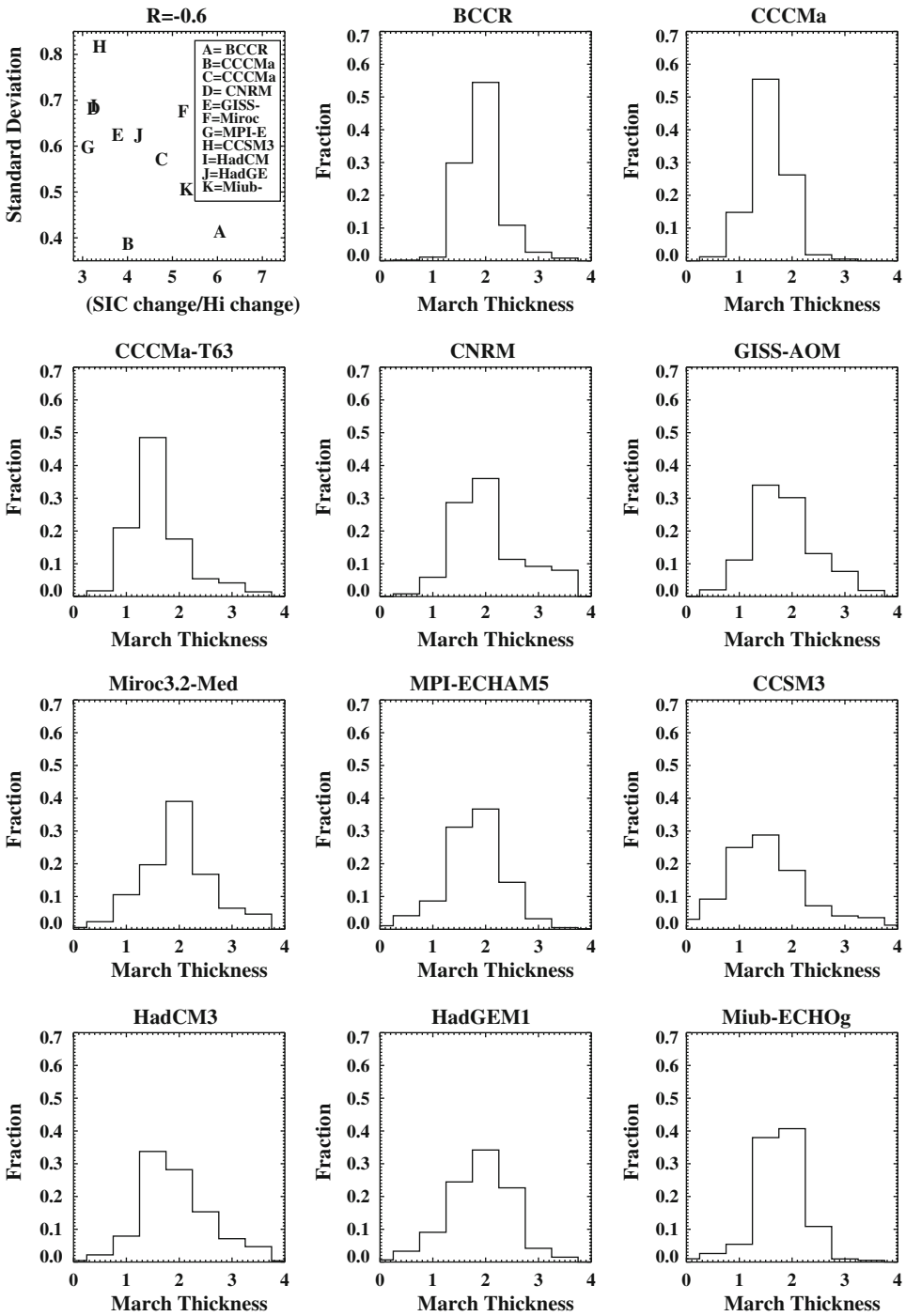

Fig. 13 *Upper left panel* scatter plot of the change in September ice concentration per ice thickness change versus the SD of the March ice thickness distribution for the different models. The change values are calculated for ice from 1.0 to 1.6 m in annual average thickness and the distribution is computed for ice with a mean thickness of approximately 1.2 m. (Remaining panels) Histograms of the fractional area of March ice within different ice thickness bins for different models. The distribution is computed for the time when the annual mean ice thickness is approximately 1.2 m. Only the 11 models which have ice thickness that varies from 1.6 to 1.0 m are evaluated

Over the twenty-first century, all models show a decrease in ice volume resulting from increased annual net melt (melt exceeding growth), partially compensated by reduced ice loss via transport to lower latitudes (i.e., reduced divergence). The magnitudes and relative importance of the ice melt and growth terms that determine the net value nevertheless vary considerably. These ice mass budget changes are related to the initial and evolving ice state. Models with thicker initial (mid twentieth century) sea ice generally have larger ice volume loss. Additionally, the relative balance of changes in ice melt and growth are strongly associated with the evolving late-summer extent. Inter-model scatter in the evolving surface heat fluxes are also related to the sea ice mass loss. Models with larger increases in net ice melt are typically those with larger increases in absorbed shortwave radiation and larger increases in the incident longwave flux. This in turn invokes consideration of different strengths in cloud radiative forcing and albedo feedbacks.

A number of factors appear to govern how the changing sea ice mass budgets translate into reductions in September ice extent. Models with initially thicker, more extensive ice cover generally retain more extensive summer sea ice throughout the twenty-first century even though they simulate larger increases in net ice melt. That a number of the models have fairly thick initial ice cover helps to explain the slower simulated decline in ice extent relative to observations (Stroeve et al. 2007). Also important is the simulated thickness distribution. Models with smaller summer ice retreat per meter of mean ice thickness loss typically have a larger spread in the spring ice thickness distribution, suggesting a stabilizing effect by thick ice regions. Although not explicitly addressed here, this also suggests that the presence and properties of a sub-gridscale ice thickness distribution, as included in a number of models, influences how changes in sea ice mass budgets translate into ice extent loss. These factors contribute to a large range in the projected timing of the transition from a perennial to seasonal Arctic ice cover.

Our analysis of the CMIP3 models suggests that obtaining reasonable twenty-first century projections of Arctic sea ice conditions, including the timing at which a seasonally ice-free ocean might be realized, requires reasonable simulations of at least: (1) present day ice conditions, including extent and the spatial distribution of ice thickness; (2) the evolving surface energy budget and its consequent influence on the sea ice mass budget; (3) the change in ice area per ice thickness change. To achieve this involves numerous and interacting factors across the coupled system. Projected onset of seasonally ice-free conditions of course also depends on uncertainties in the external forcing used to drive the models (e.g. the scenario of greenhouse gas concentration change and timing of future volcanic eruptions).

While these simulation requirements are strongly interrelated, direct observations for model evaluation are often sparse. Our study suggests that albedo and cloud processes merit particular attention. While issues of ocean heat transport and ice–ocean exchange also appear important, direct observations for evaluation are especially scanty. In general, an assessment of an individual model's simulated mean sea ice climate state and its inherent internal variability provides some indication on how well that model is likely to simulate sea ice loss through the twenty-first century.

Acknowledgments This study was supported by NASA grant NNG06GB26G and NSF grant ARC-0531040. We acknowledge the modeling groups, the Program for Climate Model Diagnosis and Intercomparison (PCMDI) and the WCRP's Working Group on Coupled Modelling (WGCM) for their roles in making available the WCRP CMIP3 multi-model dataset. Support of this dataset is provided by the Office of Science, US Department of Energy. NCAR is supported by the National Science Foundation.

References

ACIA (2005) Impacts of a warming Arctic. Arctic Climate Impact Assessment (ACIA). Cambridge University Press, Cambridge, 140 pp

Arzel O, Fichefet T, Goosse H (2006) Sea ice evolution over the 20th and 21st centuries as simulated by current AOGCMs. Ocean Model 12:401–415. doi:10.1016/j.ocemod.2005.08.002

Arzel O, Fichefet T, Goosse H, Dufresne J-L (2008) Causes and impacts of changes in the Arctic freshwater budget during the 20th and 21st centuries in an AOGCM. Clim Dyn 30:37–58. doi:10.1007/s00382-007-0258-5

Belchansky GI, Douglas DC, Platonov NG (2004) Duration of the Arctic sea ice melt season: regional and interannual variability, 1979–2001. J Clim 17:67–80. doi:10.1175/1520-0442(2004)017<0067:DOTASI>2.0.CO;2

Bitz CM, Roe GH (2004) A mechanism for the high rate of sea-ice thinning in the Arctic Ocean. J Clim 17:3622–3631. doi:10.1175/1520-0442(2004)017<3623:AMFTHR>2.0.CO;2

Bitz CM, Gent PR, Woodgate RA, Holland MM, Lindsay R (2006) The influence of sea ice on ocean heat uptake in response to increasing CO_2. J Clim 19:2437–2450. doi:10.1175/JCLI3756.1

Bourke RH, Garrett RP (1987) Sea ice thickness distribution in the Arctic Ocean. Cold Reg Sci Technol 13:259–280. doi:10.1016/0165-232X(87)90007-3

Chapman WL, Walsh JE (2007) Simulations of Arctic temperature and pressure by global coupled models. J Clim 20:609–632. doi:10.175/JCLI4026.1

DeWeaver ET, Hunke EC, Holland MM (2008) Comment on "On the reliability of simulated Arctic sea ice in global climate models'' by I. Eisenman, N. Untersteiner, and J. S. Wettlaufer. Geophys Res Lett 35:L04501. doi:10.1029/2007GL031325

Gerdes R, Koberle C (2007) Comparison of Arctic sea ice thickness variability in IPCC climate of the 20th century experiments and in ocean–sea ice hindcasts. J Geophys Res 112:C04S13. doi:10.1029/2006JC003616

Gorodetskaya IV, Tremblay LB, Liepert B, Cane MA, Cullather RI (2008) The influence of cloud and surface properties on the Arctic Ocean shortwave radiation budget in coupled models. J Clim 21. doi:10.1175/2007JCLI1614.1

Holland MM, Bitz CM (2003) Polar amplification of climate change in coupled models. Clim Dyn 21:221–232. doi:00382-003-0332-6

Holland MM, Bitz CM, Tremblay B (2006a) Future abrupt reductions in the Summer Arctic sea ice. Geophys Res Lett 33:L23503. doi:10.1029/2006GL028024

Holland MM, Bitz CM, Hunke EC, Lipscomb WH, Schramm JL (2006b) Influence of the sea ice thickness distribution on Polar Climate in CCSM3. J Clim 19:2398–2414. doi:10.1175/JCLI3751.1

Houghton JT et al (eds) (2001) Climate change 2001: the scientific basis, Cambridge University Press, Cambridge

IPCC (2007) Climate change 2007: the physical science basis. In: Solomon SD, Qin M, Manning ZC, Marquis M, Averyt KB, Tignor M, Miller HL (eds) Contribution of Working Group I to the Fourth Assessment Report of the Intergovernmental Panel on Climate Change. Cambridge University Press, Cambridge, 996 pp

Manabe S, Stouffer RJ (1980) Sensitivity of a global climate model to an increase of CO_2 in the atmosphere. J Geophys Res 85(C10):5529–5554. doi:10.1029/JC085iC10p05529

Maslanik JA, Fowler C, Stroeve J, Drobot S, Zwally HJ, Yi D, Emery WJ (2007) A younger, thinner ice cover: increased potential for rapid, extensive ice loss. Geophys Res Lett 34:L24501. doi:10.1029/2007GL032043

Maykut G (1982) Large-scale heat exchange and ice production in the Central Arctic. J Geophys Res 87:7971–7984. doi:10.1029/JC087iC10p07971

Maykut GA (1986) The surface heat and mass balance. In: Untersteiner N (ed) The geophysics of sea ice. Plenum Press, New York, pp 395–464

Meehl GA, Covey C, Delworth T, Latif M, McAvaney B, Mitchell JFB, Stouffer R, Taylor KE (2007) THE WCRP CMIP3 multimodel dataset: a new era in climate change research. Bull Am Meteorol Soc 88. doi:10.1175/BAMS-88-9-1383

Nghiem SV, Chao Y, Neumann G, Li P, Perovich DK, Street T, Clemente-Colon P (2006) Depletion of perennial sea ice in the East Arctic Ocean. Geophys Res Lett 33:L17501. doi:10.1029/2006GL027198

Overland JE, Spillane MC, Soreide NN (2004) Integrated analysis of physical and biological pan-Arctic change. Clim Change 63:291–322. doi:10.1023/B:CLIM.0000018512.40506.d2

Rothrock DA, Yu Y, Maykut GA (1999) Thinning of the Arctic sea-ice cover. Geophys Res Lett 26:3469–3472. doi:10.1029/1999GL010863

Serreze MC et al (2000) Observational evidence of recent change in the northern high-latitude environment. Clim Change 46:159–207. doi:10.1023/A:1005504031923

Serreze MC et al (2003) A record minimum arctic sea ice extent, area in 2002. Geophys Res Lett 30:1110. doi:10.1029/2002GL016406

Serreze MC, Francis JA (2006) The Arctic amplification debate. Clim Change. doi:10.10007/s10584-005-9017

Serreze MC, Holland MM, Stroeve J (2007a) Perspectives on the Arctic's shrinking sea-ice cover. Science 315:1533–1536. doi:10.1126/science.1139426

Serreze MC, Barrett AP, Slater AG, Steele M, Zhang J, Trenberth KE (2007b) The large-scale energy budget of the Arctic. J Geophys Res 112. doi:10.1029/2006JD008230

Sorteberg A, Kattsov V, Walsh JE, Pavlova T (2007) The Arctic surface energy budget as simulated with the IPCC AR4 AOGCMs. Clim Dyn 29. doi:10.1007/s00382-006-0222-9

Stroeve JC, Serreze MC, Fetterer F, Arbetter T, Meier M, Maslanik J, Knowles K (2005) Tracking the Arctic's shrinking ice cover: another extreme September minimum in 2004. Geophys Res Lett 32:L04501. doi:10.1029/2004GL021810

Stroeve J, Holland MM, Meier W, Scambos T, Serreze MC (2007) Arctic Sea Ice Decline: Faster than Forecast. Geophys Res Lett 34. doi:10.1029/2007GL029703

Stroeve J, Serreze M, Drobot S, Gearhead S, Holland M, Maslanik J, Meier W, Scambos T (2008) Arctic sea ice plummets in 2007. EOS 89(2):13–14. doi:10.1029/2008EO020001

Vavrus S, Waliser D, Schweiger A, Francis J (2008) Simulations of 20th and 21st century Arctic clouds in the global climate models assessed in the IPCC AR4. Clim Dyn (submitted)

Winton M (2006) Does the Arctic sea ice have a tipping point? Geophys Res Lett 33. doi:10.1029/2006GL028017

Zhang X, Walsh JE (2006) Toward a seasonally ice-covered Arctic Ocean: scenarios from the IPCC AR4 model simulations. J Clim 19:1730–1747. doi:10.1175/JCLI3767.1